



Iron-based metal-organic frameworks integrated into 3D printed ceramic architectures

Alma D. Salazar-Aguilar^{a,b,c}, Asunción Quintanilla^b, Sofía M. Vega-Díaz^a, José A. Casas^b, Pilar Miranzo^c, M. Isabel Osendi^c, Manuel Belmonte^{c,*}

^a Departamento de Ingeniería Química, Tecnológico Nacional de México, Instituto Tecnológico de Celaya, Av. García Cubas Pte # 600 esq. Avenida Tecnológico, Celaya, Guanajuato, 38010, Mexico

^b Chemical Engineering Department, Universidad Autónoma de Madrid, Ctra. Colmenar km 15, Madrid, 28049, Spain

^c Institute of Ceramics and Glass (ICV-CSIC), Campus de Cantoblanco, Kelsen 5, Madrid, 28049, Spain

ARTICLE INFO

Keywords:

3D printing
MOF
Ceramics
Catalysis
Selective oxidation
Phenol

ABSTRACT

The promising applications of metal-organic frameworks (MOF) can be widened if these materials were additive manufactured to develop three-dimensional (3D) MOF architectures. In this work, iron-based MOF/silicon carbide (SiC) composite aqueous inks with a high solids content (64 wt%) are printed into 3D periodic lattices by a direct ink writing technique (Robocasting). MOF appear fully integrated within the cellular architectures, which display total porosities in the range of 74–78% depending on the scaffold design. The 3D MOF-Fe/SiC structures exhibit good mechanical strength (~4.6 MPa) and a semiconductor-like behaviour. The structures show a remarkable response in the hydroxylation of phenol with hydrogen peroxide, demonstrating high selectivity and yield to dihydroxybenzene species.

1. Introduction

Metal-organic frameworks (MOF) are porous materials formed by metal ions/clusters and organic linkers that have attracted a great interest during the last years due to their excellent physicochemical properties that make them promising materials for a wide range of applications, including, among others, catalysis, chemical sensing, gas separation or biomedicine [1,2]. On the other hand, the rise of the additive manufacturing technologies in the last decades for developing 3D structures with a precise control of their sizes and shapes has encouraged the research activities aimed to produce 3D printed catalysts [3,4]. The 3D structured catalysts offer the benefits of easy handling and potential enhancements of key properties such as the fluid permeability and the mass and heat transfers. In this sense, at present, two approaches have been intended to produce 3D MOF-based catalysts. One of them consists in coating a 3D printed cellular support, typically a polymer monolith, with MOF particles that are in-situ grown on the scaffold surface [5,6]. These 3D MOF have been employed to decompose organic dyes based on the Fenton reaction with both good catalytic degradation efficiency and good reaction rate constant, although the MOF coating could be fast removed, limiting its catalytic performance.

A second and more challenging approach involves the deep integration of the MOF inside the 3D printed structure by developing a MOF-based ink printable using direct ink writing (DIW) methods. Nowadays, there are only few works addressing the DIW of 3D MOF structures. In this way, Thakkar et al. [7] manufactured 3D MOF-Co and MOF-Ni from a deionized water/ethanol-based ink containing the MOF powders and some additions of bentonite and polyvinyl alcohol for colloidal stabilization of the ink. The MOF monoliths were employed for CO₂ adsorption and exhibited comparable results to those of MOF powders. Young et al. [8] printed 3D MOF-Zr structures using an acrylate-based ink, removing the organic binders by thermal treatment and, afterwards, tested them to produce the catalytic breakdown of a nerve agent simulant methyl-paraoxon. Lim et al. [9] developed a 3D MOF-Cu from a printable colloidal gel that was employed for methane adsorption with promising results. Lyu et al. [10] reported the printing of 3D MOF-Co monoliths from an ink containing a high amount of surfactant (Pluronic F127), which were further annealed to create a cobalt-carbon porous framework to be employed in Li–O₂ batteries. Finally, Dhainaut et al. [11] manufactured different 3D MOF (Cu, Ni, Zr) structures from cellulose-based inks that were employed for high-pressure methane storage or ethane/ethylene separation with performances comparable to those of their

* Corresponding author.

E-mail address: mbelmonte@icv.csic.es (M. Belmonte).

<https://doi.org/10.1016/j.oceram.2020.100047>

Received 27 October 2020; Received in revised form 9 December 2020; Accepted 14 December 2020

Available online 16 December 2020

2666-5395/© 2020 The Authors. Published by Elsevier Ltd on behalf of European Ceramic Society. This is an open access article under the CC BY-NC-ND license

(<http://creativecommons.org/licenses/by-nc-nd/4.0/>).

powder counterparts.

In the present work, silicon carbide (SiC) ceramics were filled by as-synthesized MOF-Fe powders. The goal was to develop a printable aqueous MOF-Fe/SiC composite ink with low organic contents, and to manufacture, in a next step, 3D MOF-Fe/SiC cellular architectures by DIW (Robocasting). The MOF-Fe/SiC system was selected attending to the following considerations: i) SiC is an excellent support to provide to the monoliths robustness and chemical resistance in harsh environments, ii) Fe is a common catalyst for oxidation reactions, especially when the oxidant is hydrogen peroxide (H_2O_2), and iii) the fast decomposition of H_2O_2 into the powerful oxidant species $\text{HO}\bullet$ on the Fe sites would avoid unnecessary high contents of MOF-Fe (commercially expensive or with a laborious synthesis at lab-scale) into the 3D printed structures.

The microstructure of the 3D MOF-Fe/SiC cellular architectures was fully characterized and properties such as the compressive strength and electrical conductivity were also estimated. Besides, the catalytic performance of the monoliths in the selective oxidation of hydrocarbons, a key industrial reaction [12], was investigated by considering the hydroxylation of phenol with H_2O_2 as target reaction, attending to the promising results previously achieved with MOF-Fe powders [13].

2. Experimental procedure

MOF powders containing a 20 wt% of Fe nanoparticles were synthesized at room temperature by mixing iron chloride (FeCl_3 , Sigma Aldrich) and trimesic acid (H_3BTC , Sigma Aldrich) in a water solution. The detailed description of the procedure can be found elsewhere [13]. The dried powders were sonicated for 1 h in ethanol to avoid the formation of MOF agglomerates. In parallel, an ethanol solution containing SiC nanoparticles (0.5 wt% of iron impurities, Nanostructured & Amorphous Materials Inc. -NanoAmor-, mean particle size of ~ 50 nm) was ball milled for 0.5 h using Teflon balls. When both processes finished, the ethanol solutions were mixed and ball milled for 2 h. Afterwards, the solvent was removed in a rotary-evaporator at 90°C , and the powder mixture was dried at 100°C for 12 h and sieved through a $63\ \mu\text{m}$ mesh. The weight ratio (in %) of the MOF:SiC composition was 2.5:97.5. The total iron content of the powder mixture was 1.0 wt%.

The basis of the ink composition was similar to that previously developed for plain SiC inks by some of the present authors [14], which contained the following organics: high molecular weight polyethylenimine (H-PEI, PEI 25000, Sigma Aldrich; <1 wt% of water content), low molecular weight polyethylenimine (L-PEI, PEI 2000, Sigma Aldrich; 50 wt% of water content), both used as dispersants to enhance the solid contents by means of electrostatic repulsions, and hydroxypropyl methylcellulose (MC, Methocel F4M, Dow Chemical Co.; 95 wt% of water content) to act as viscosifier and promote the formation of a gel. For the present ink, in order to achieve the necessary viscoelastic behaviour and high storage modulus of the MOF-Fe/SiC ink, the amount of these organics was conveniently adapted and, at the same time, ammonium polyacrylate (APA, DARVAN 821-A, Vanderbilt Minerals; 60 wt% of water content) was also added as flocculant to enhance the rigidity of the printed filaments. The MOF-Fe/SiC powders, deionized water and organics were sequentially added and homogenized at 2000 rpm for 30 s in a planetary centrifugal mixer (ARE-250, Thinky Co.) that contained Si_3N_4 milling balls. The apparent viscosity (η) versus the shear rate ($\dot{\gamma}$), and the shear storage (G') and loss (G'') moduli as a function of the shear stress (τ) were measured with a rheometer (CVO 100 D, Bohlin Instruments) equipped with a cone-and-plate geometry (diameter: 40 mm; cone angle: 4°).

3D MOF-Fe/SiC periodic lattices were computer designed (RoboCAD 4.0, 3-D Inks LLC), in particular, cuboids with 24 layers ($12 \times 12 \times 6\ \text{mm}^3$) and cylinders with 20 layers (14 mm of diameter and 5 mm of height). In both cases, the lattices contained a linear array of parallel filaments in the x-y plane, each array rotated 90° respect to the adjacent layers. Then, the structures were printed with needles of $330\ \mu\text{m}$ inner diameter onto a flat alumina substrate using a custom three-axis

robocasting system (A-3200, 3-D Inks LLC) and a X-Y table velocity of $10\ \text{mm s}^{-1}$.

Thermogravimetric-differential thermal analysis (TGA-DTA, SDT Q600, TA Instruments) of the printed scaffolds was performed to establish the most suitable thermal treatment to remove the organics added to the ink, avoiding at the same time the damage of the MOF-Fe structure. These analysis were conducted in air up to 1000°C and a heating rate of $5^\circ\text{C}\cdot\text{min}^{-1}$. The thermally treated 3D structures were characterized by X-ray diffraction (XRD, Bruker D5000, Siemens), optical stereomicroscopy (Nikon SMZ1000), field emission scanning electron microscopy (FESEM, Hitachi S-4700), specific surface area measurements (S_{BET} , Micromeritics Tristar 3000 apparatus), and total reflection X-ray fluorescence (TXRF EXTRA II, Rich & Seifert). In addition, the geometrical density (ρ_{geo}) was calculated from the weight and dimensions of the treated scaffolds; while the bulk density (ρ_{bulk}) was assessed by the Archimedes' method. Considering that the theoretical density of MOF-Fe/SiC composition is $\sim 3.22\ \text{g cm}^{-3}$, the total porosity (π_{total}), as sum of the porosity of the patterned channels and the skeleton, and the rod porosity (π_{rod}) were estimated from ρ_{geo} and ρ_{bulk} data, respectively.

The compression strength (σ_c) of the MOF-Fe/SiC cuboids and cylinders was estimated using a universal testing machine (ZwickiLine Z5.0 TS, Zwick-Roell) with a 5 kN load cell (load cell error $\pm 0.5\%$) and a displacement rate of $0.5\ \text{mm min}^{-1}$. At least four scaffolds were compression tested at their patterned sides. The effective electrical conductivity (σ_{eff}) of the cuboids was assessed in the longitudinal direction, where the current mainly flows along the struts, by the four-probe DC method (potentiostat/galvanostat, Autolab PGSTAT302 N). The current flow varied between 100 and 3000 mA and the σ_{eff} was calculated using the following expression: $\sigma_{\text{eff}} = l/(A \times R)$, being l the distance between the inner electrodes, A the apparent transversal area of the scaffold structure, and R the resistance obtained from the slope of the current-voltage plot.

The phenol hydroxylation experiments were carried out batch-wise in the monolithic stirrer reactor (see discussion section). The standard testing conditions were atmospheric pressure, temperature of 25°C and water (Milli-Q ultrapure water) as unique solvent. The stirrer speed of the monolithic impeller was fixed at 300 rpm and the mass of the two pieces of 3D MOF-Fe/SiC monoliths attached to the stirrer shaft was 0.95 g. In a typical experiment, the reactor was filled with 400 mL of 0.35 M phenol solution and, once the desired reaction temperature was reached (IKA RCT basic) under stirring, a volume of an adjusted concentration of H_2O_2 was fed by a three-pulse dosage along the reaction (5 mL at 0, 80 and 160 min of reaction). The Fe concentration, $[\text{Fe}]_{3\text{D}}$, was $0.02\ \text{g L}^{-1}$, and the phenol to H_2O_2 and the phenol to Fe molar ratios were equal to 1:1 and 857:1, respectively. The performance of the catalyst was evaluated in terms of conversion, selectivity and yield. These variables have been defined in the Supporting Information.

The progress of the reaction was followed by monitoring the concentration of phenol and the oxidized species, viz. catechol (CTL), hydroquinone (HQ), *p*-benzoquinone (BQ) and resorcinol (RSL), by high performance liquid chromatography (Ultimate 3000, Thermo Scientific, C18 $5\ \mu\text{m}$ column $150 \times 4.6\ \text{mm}$, 4 mM H_2SO_4 as mobile phase, DAD detector at wavelengths of 210 and 246 nm). Total organic carbon (TOC) was quantified with a TOC analyser (Shimadzu TOC VSCH). H_2O_2 concentration was obtained by colorimetric titration TiOSO_4 method (UV2100 Shimadzu UV-vis spectrophotometer) [15]. The content of Fe in solution was measured by TXRF (S2 PicoFox Bruker).

3. Results and discussion

The rheological study of the developed MOF-Fe/SiC ink evidenced its excellent colloidal properties for the DIW process. In particular, the ink exhibited pseudoplastic behaviour, decreasing the apparent viscosity in about three orders of magnitude as the shear rate increased (Fig. 1a). This response allows injecting (high shear rate-low viscosity) the MOF-Fe/SiC ink through the nozzle tip, keeping the filamentary shaping when it left the tip (low shear rate-high viscosity). Fig. 1b also confirms the high

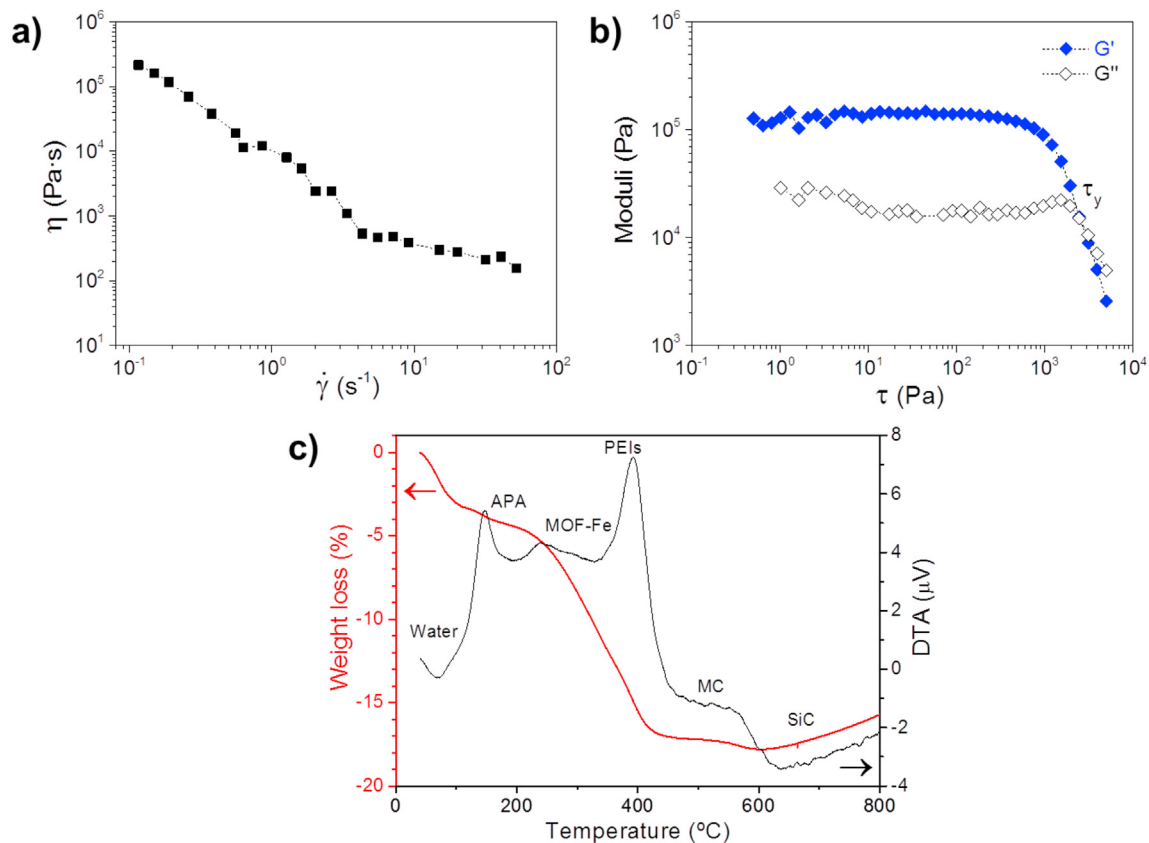


Fig. 1. a) Apparent viscosity (η) versus shear rate ($\dot{\gamma}$) and b) shear storage (G') and loss (G'') moduli versus shear stress (τ) of the MOF-Fe/SiC ink. c) DTA/TGA (weight loss) plot of the as-printed 3D MOF-Fe/SiC structure, remarking the decomposition of the ink components.

storage modulus of the ink ($G' \sim 10^5$ Pa), which is above the loss modulus ($G'' \sim 10^4$ Pa) until they crossed at a high yield stress value ($\tau_y \sim 2.5 \times 10^3$ Pa). The printed scaffolds, both rectangular prisms and cylinders, were formed by an array of parallel filaments (Fig. 2a) without any evident sign of deformation (Fig. 2b), thus confirming the expected

printability considering its high G' and τ_y data, as G. V. Franks' studies about the printability of ceramic structures also predict [16]. As result of the rheological study, the tuned MOF-Fe/SiC ink composition was (in wt.%) 64.0 MOF-Fe/SiC composite; 25.4 deionized water; 3.3 H-PEI, 3.2 L-PEI, 3.2 MC and 0.9 APA, that corresponds in vol% to 35.8

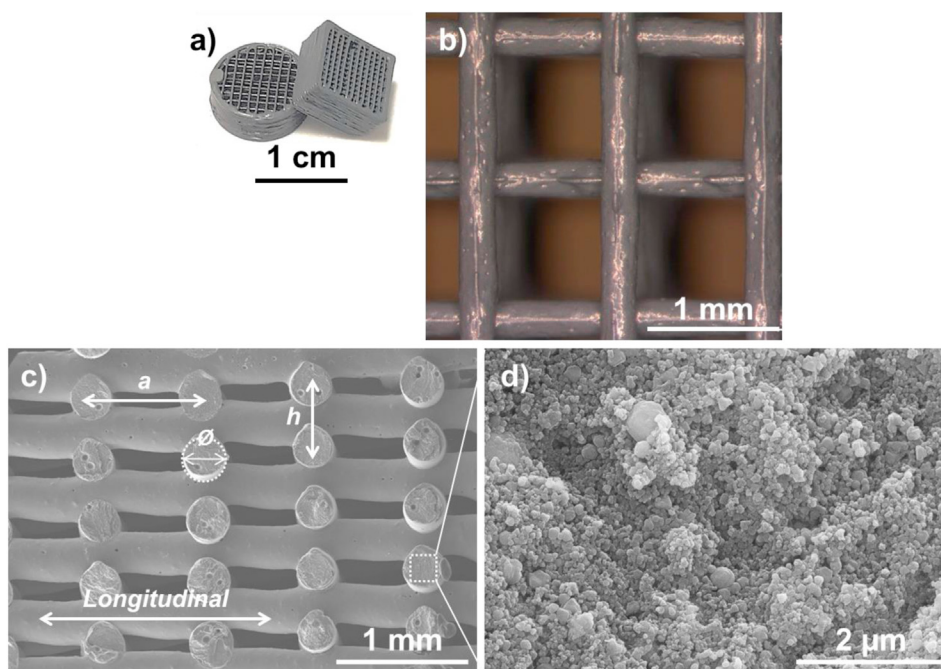


Fig. 2. a) Examples of as-printed rectangular prismatic and cylindrical MOF-Fe/SiC scaffolds. b) Optical image showing a detail of the cell side of the patterned structure in a cylinder. c) FESEM micrograph of the cross-section view of a cylindrical scaffold after the heat treatment at 250 °C, pointing the longitudinal direction and the cell parameters such as mean rod diameter (ϕ), in-plane distance between two adjacent rods (a), and distance between two equivalent layers in the z-direction (h). d) Microstructure inside a strut taken in the frame highlighted in c).

MOF-Fe/SiC, 55.1 water (including deionized water plus water of the organics) and 9.1 pure organics.

The DTA/TGA analysis of the as-printed structures (Fig. 1c) revealed the sequence of the decomposition of their different components with the temperature. In this sense, water and APA were removed below 250 °C, PEIs and MC were burnt-out between 300 and 575 °C, and the oxidation of SiC occurred at temperatures above 600 °C. The most critical issue is the thermal stability of the MOF-Fe structure because the decomposition of the trimesic acid ligands typically takes place at ~300 °C [13]. Therefore, the MOF-Fe/SiC monoliths were heat treated in air at 250 °C for 1 h (heating and cooling rates of 3 °C·min⁻¹) to remove just water and APA while keeping unchanged the MOF-Fe for the catalytic applications.

The heat treated 3D structures had a specific surface area of 20 m² g⁻¹, and the fracture surface view of the cross-section (Fig. 2c) showed an excellent integrity of the printed layers, maintaining the patterned design even after the removal of the water and some of the organics. In terms of density and porosity, prisms and cylinders had a ρ_{geo} of 0.83 ± 0.03 g cm⁻³ and 0.72 ± 0.03 g cm⁻³, respectively; which correlates with their differences in the CAD designs, as the density of the MOF-Fe/SiC skeletons was almost identical (ρ_{bulk} of 1.37 ± 0.08 g cm⁻³ for prisms and 1.38 ± 0.05 g cm⁻³ for cylinders). Regarding the porosity, π_{total} of the prisms and cylinders was $74 \pm 1\%$ and $78 \pm 1\%$, respectively; whereas π_{rod} for prisms was $58 \pm 3\%$ and $57 \pm 2\%$ for cylinders. Finally, the porosity of the 3D CAD structure (π_{3D}) was $51 \pm 5\%$ for prisms and $54 \pm 5\%$ for cylinders.

The compressive tests for both monolith geometries (Fig. 3a) evidenced the common response of cellular materials, i.e., the presence of an initial linear elastic region where the structure deformed under the applied load until reached a maximum in the curve, followed by a gradual decrease of the stress as the strain progressed until the collapse of the scaffold (Fig. 3a). The sharp peaks observed in the elastic regime would be associated to the fracture of some struts, although the printed structure did not catastrophically fail from these events and was able to bear load even after the peak stress. The maximum compressive stress value corresponds to the crushing strength (σ_c), being 4.4 ± 0.5 MPa (strain = $4.1 \pm 0.4\%$) and 4.7 ± 0.3 MPa (strain = $5.4 \pm 0.7\%$) for cylinders and prisms, respectively. Comparing with the scarce mechanical data of 3D printed MOF-based structures reported until now [7,11], the present monoliths exhibited a highly advantageous robustness. In fact, the current σ_c values are about one order of magnitude higher than those reported by Thakkar et al. [7] for 3D MOF-Ni ($\sigma_c = 0.48$ MPa) and MOF-Co ($\sigma_c = 0.56$ MPa), although the total porosity of these structures was not provided, which makes difficult a real comparison. However, this exercise can be done with data reported by Dhainaut et al. [11]. These authors found that all 3D printed MOF structures were mechanically stable, reaching σ_c up to 0.6 MPa for a relative density of ~0.30, which is

a strength value around one order of magnitude lower than that obtained for the current monoliths with relative densities quite similar (0.22 for cylinders and 0.25 for prisms). This enhanced mechanical resistance would be explained by the high solids content of the ink, its excellent rheological performance and the strengthening provided by the SiC nanoparticles.

Fig. 3b depicts I-V data of heat treated prisms using the four-probe DC method (see inset in the figure). Taking the electrical resistance from the slope of the fitted line ($R^2 = 0.9997$), the electrical conductivity in the longitudinal direction was assessed to be 7.0 S m⁻¹. This value confirms that the scaffold is slightly conductor despite the organic ligands of the MOF-Fe structure would decrease the conductivity. In addition, it is possible to estimate the intrinsic electrical conductivity of the MOF-Fe/SiC rods ($\sigma_{\text{e,rod}}$) using a resistor model reported by some of the present authors [17], and known some cell parameters of the monoliths, as follows:

$$\sigma_{\text{e,rod}} = \frac{2a}{\varnothing} \sigma_{\text{eff-L}} \quad (2)$$

where a is the distance between two adjacent struts (843 ± 23 μm in the present case for heat treated prisms), \varnothing is the mean diameter of the struts (320 ± 10 μm) and $\sigma_{\text{eff-L}}$ is the electrical conductivity of the scaffold along the longitudinal direction. From these equation, a $\sigma_{\text{e,rod}}$ value of 37 S m⁻¹ was obtained. This electrical response could be potentially beneficial for removing organics adsorbed into the scaffold by Joule heating [18].

The catalytic performance of the 3D MOF-Fe/SiC monoliths was evaluated in the hydroxylation of phenol using the monolithic stirrer reactor (Fig. 4a). The results obtained are provided in Fig. 4b and c, along with those obtained in presence of the MOF-Fe powders under the same standard operating conditions and phenol conversion ($X_{\text{phenol}} = 25\%$), though with twice the Fe concentration, $[\text{Fe}]_{\text{powder}} = 0.04$ g L⁻¹ [13]. Fig. 4b collects the efficiency of the H₂O₂ consumption ($\text{H}_2\text{O}_{2\text{eff}}$), phenol selectivity to HQ (S_{HQ}) and CTL (S_{CTL}) and phenol yield to both dihydroxybenzenes ($Y_{\text{DHBZ}} = \text{CTL} + \text{HQ}$). As it can be observed, the 3D MOF-Fe/SiC monoliths exhibited a higher selectivity to HQ and CTL and a higher yield to DHBZ than the MOF-Fe powders. In fact, unprecedented values for S_{DHBZ} and Y_{DHBZ} , equal to 80 and 20%, respectively, are here reported (Fig. 4b) for a solid catalyst at room conditions. In addition, the low presence of adsorbed species in the 3D monoliths was also remarkable (Fig. 4c), which is a fact that favours the efficiency consumption of H₂O₂. This is explained by the low specific surface area available for the adsorption on the 3D monoliths ($S_{\text{BET}} = 20$ m² g⁻¹), compared to that of the powders ($S_{\text{BET}} = 975$ m² g⁻¹).

Regarding the catalytic activity, the 3D MOF-Fe/SiC monolith was less active than the counterpart powder. Actually, significant longer reaction times were required in the monoliths to achieve the same X_{phenol} of

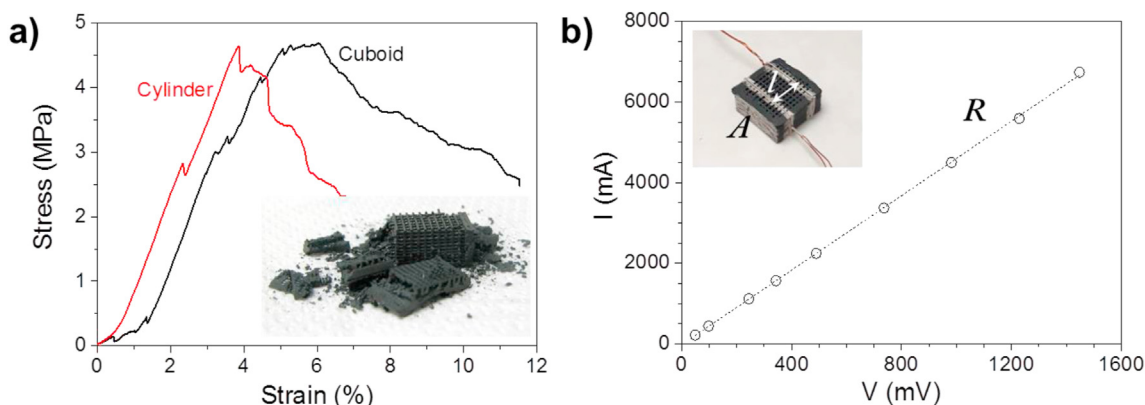


Fig. 3. a) Representative stress-strain curves for heat treated MOF-Fe/SiC prisms and cylinders. The inset shows an image of a collapsed prism after the compressive test on the cell-side. b) Current-voltage plot recorded through the longitudinal direction of the scaffold (see inset), including their main parameters (A , R and I) to determine the effective electrical conductivity.

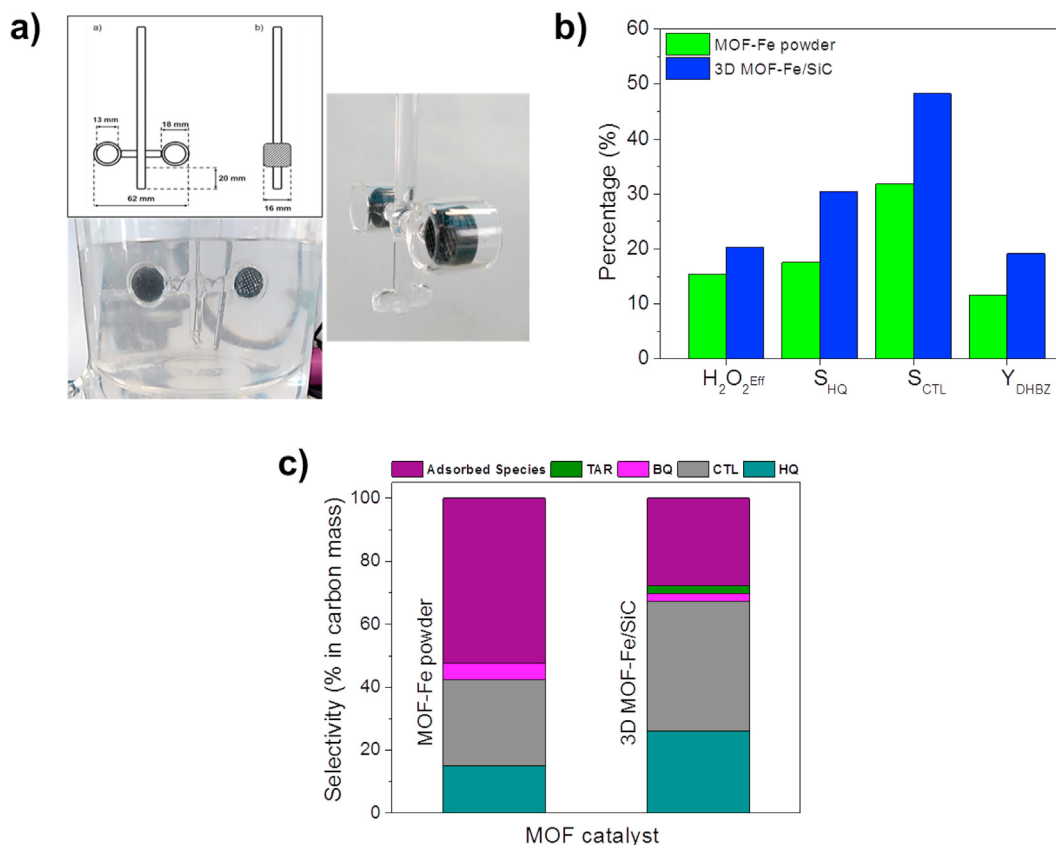


Fig. 4. a) The experimental set-up of the monolithic stirrer reactor used in the hydroxylation of phenol, and drawing with the dimensions of the stirrer and MOF-Fe/SiC monoliths placed into the stirrer reactor. b) Catalytic performance and c) carbon mass distribution at $X_{phenol} = 25\%$. The results in presence of the MOF powders are included for the sake of comparison also at $X_{phenol} = 25\%$. Operating conditions: $[Phenol]_0 = 0.35 \text{ mol L}^{-1}$, $[H_2O_2]_0 = 0.35 \text{ mol L}^{-1}$, $[Fe]_{3D} = 0.02 \text{ g L}^{-1}$, $[Fe]_{powder} = 0.04 \text{ g L}^{-1}$, $T = 25^\circ \text{C}$.

25% than in the MOF-Fe powder (24 vs. 1 h, respectively). It is the low H_2O_2 decomposition rate and, consequently, the slow availability of the oxidant $HO\bullet$ species in presence of the 3D MOF-Fe/SiC monoliths, the reason for the poor over-oxidation of phenol into *p*-benzoquinone and tar by products and, hence, the prominent selectivity that the monoliths show towards the dihydroxybenzene species.

4. Conclusions

3D cellular MOF-Fe/SiC rectangular prisms and cylinders have been direct ink written from aqueous pseudoplastic inks containing a high solid loading (64 wt%). The heat treated 3D structures keep MOF-Fe fully integrated into the scaffolds, which are slightly electrical conductors and exhibit high robustness, reaching compressive strengths of $\sim 4.6 \text{ MPa}$ for monoliths with densities in the range of $0.72\text{--}0.83 \text{ g cm}^{-3}$. 3D MOF-Fe/SiC structures present a good catalytic performance in the hydroxylation of phenol, especially in the selectivity (80%) and yield (20%) to dihydroxybenzene, higher values than those obtained for MOF-Fe powders. This response of the monoliths is favoured by controlling the dosing of hydrogen peroxide that also allows considerably reducing the production of undesired by-products. These results encourage the use of 3D printing technologies for manufacturing novel catalytic MOF-based architectures.

Declaration of competing interest

The authors declare that they have no known competing financial interests or personal relationships that could have appeared to influence the work reported in this paper.

Acknowledgements

This work was supported by the following funding organisms and projects: Spanish Government under the project RTI2018-095052-BI00 (MICINN/AEI/FEDER, UE), Community of Madrid under the project S2018/EMT-4341, CSIC project I-COOP+ 2019 (Ref. COOPB20405), TNM projects 7936.20-P and 9063.20-P, and CONACYT under the project 764635. Authors thank Dr. D. Pérez-Coll for his experimental assistance in the electrical measurements.

Appendix A. Supplementary data

Supplementary data to this article can be found online at <https://doi.org/10.1016/j.oceram.2020.100047>.

References

- [1] S. Yuan, L. Feng, K. Wang, J. Pang, M. Bosch, C. Lollar, Y. Sun, J. Qin, X. Yang, P. Zhang, Q. Wang, L. Zou, Y. Zhang, L. Zhang, Y. Fang, J. Li, H.-C. Zhou, Stable metal-organic frameworks: design, synthesis, and applications, *Adv. Mater.* 30 (2018) 1704303, <https://doi.org/10.1002/adma.201704303>.
- [2] L. Jiao, J.Y.R. Seow, W.S. Skinner, Z.U. Wang, H.-L. Jiang, Metal-organic frameworks: structures and functional applications, *Mater. Today Off.* 27 (2019) 43–68, <https://doi.org/10.1016/j.mattod.2018.10.038>.
- [3] X. Zhou, C.-J. Liu, Three-dimensional printing for catalytic applications: current status and perspectives, *Adv. Funct. Mater.* 27 (2017) 1701134, <https://doi.org/10.1002/adfm.201701134>.
- [4] C. Hurt, M. Brandt, S.S. Priya, T. Bhatelia, J. Patel, P.R. Selvakannan, S. Bhargava, Combining additive manufacturing and catalysis: a review, *Catal. Sci. Technol.* 7 (2017) 3421–3439, <https://doi.org/10.1039/C7CY00615B>.
- [5] Z. Wang, J. Wang, M. Li, K. Sun, C. Liu, Three-dimensional printed acrylonitrile with Cu-BTC metal-organic frameworks for the removal of methylene blue, *Sci. Rep.* 4 (2014) 4–10, <https://doi.org/10.1038/srep05939>.

- [6] D. Liu, P. Jiang, X. Li, J. Liu, L. Zhou, X. Wang, F. Zhou, 3D printing of metal-organic frameworks decorated hierarchical porous ceramics for high-efficiency catalytic degradation, *Chem. Eng. J.* 397 (2020) 125392, <https://doi.org/10.1016/j.cej.2020.125392>.
- [7] H. Thakkar, S. Eastman, Q. Al-Naddaf, A.A. Rownaghi, F. Rezaei, 3D-printed metal-organic framework monoliths for gas adsorption processes, *ACS Appl. Mater. Interfaces* 9 (2017) 35908–35916. <https://doi.org/10.1021/acsami.7b11626>.
- [8] A.J. Young, R. Guillet-Nicolas, E.S. Marshall, F. Kleitz, A.J. Goodhand, L.B.L. Glanville, M.R. Reithofer, J.M. Chin, Direct ink writing of catalytically active UiO-66 polymer composites, *Chem. Commun.* 55 (2019) 2190–2193. <https://doi.org/10.1039/c8cc10018g>.
- [9] G.J.H. Lim, Y. Wu, B.B. Shah, J.J. Koh, C.K. Liu, D. Zhao, A.K. Cheetham, J. Wang, J. Ding, 3D-printing of pure metal-organic framework monoliths, *ACS Mater. Lett.* 1 (2019) 147–153. <https://doi.org/10.1021/acsmaterialslett.9b00069>.
- [10] Z. Lyu, G.J.H. Lim, R. Guo, Z. Kou, T. Wang, C. Guan, J. Ding, W. Chen, J. Wang, 3D-printed MOF-derived hierarchically porous frameworks for practical high-energy density Li-O₂ batteries, *Adv. Funct. Mater.* 29 (2019) 1–8. <https://doi.org/10.1002/adfm.201806658>.
- [11] J. Dhainaut, M. Bonneau, R. Ueoka, K. Kanamori, S. Furukawa, Formulation of metal-organic framework inks for the 3D printing of robust microporous solids toward high-pressure gas storage and separation, *ACS Appl. Mater. Interfaces* 12 (2020) 10983–10992, <https://doi.org/10.1021/acsami.9b22257>.
- [12] G. Centi, F. Cavani, F. Trifirò, *Selective Oxidation by Heterogeneous Catalysis, Fundamental and Applied Catalysis*, Springer US, New York, 2012.
- [13] A.D. Salazar-Aguilar, G. Vega, J.A. Casas, S. Magdalena Vega-Díaz, F. Tristan, D. Meneses-Rodríguez, M. Belmonte, A. Quintanilla, Direct hydroxylation of phenol to dihydroxybenzenes by H₂O₂ and Fe-based metal-organic framework catalyst at room temperature, *Catalysts* 10 (2020) 172. <https://doi.org/10.3390/catal10020172>.
- [14] B. Román-Manso, A. de Pablos, M. Belmonte, M.I. Osendi, P. Miranzo, Microstructural designs of spark plasma sintered silicon carbide ceramic scaffolds, *Bol. Soc. Esp. Ceram. Vidr.* 53 (2014) 93–100. <https://doi.org/10.3989/cyv.132014>.
- [15] G. Eisenberg, Colorimetric determination of hydrogen peroxide, *Ind. Eng. Chem. Anal. Ed.* 15 (1943) 327–328, <https://doi.org/10.1021/i560117a011>.
- [16] S.S.L. Chan, M.L. Sesso, G.V. Franks, Direct ink writing of hierarchical porous alumina-stabilized emulsions: rheology and printability, *J. Am. Ceram. Soc.* 103 (2020) 5554–5566, <https://doi.org/10.1111/jace.17305>.
- [17] B. Roman-Manso, F.M. Figueiredo, B. Achiaga, R. Barea, D. Perez-Coll, A. Morelos-Gomez, M. Terrones, M.I. Osendi, M. Belmonte, P. Miranzo, Electrically functional 3D-architected graphene/SiC Composites, *Carbon* 100 (2016) 318–328, <https://doi.org/10.1016/j.carbon.2015.12.103>.
- [18] K. Wang, Y. Zeng, W. Lin, X. Yang, Y. Cao, H. Wang, F. Peng, H. Yu, Energy-efficient catalytic removal of formaldehyde enabled by precisely Joule-heated Ag/Co₃O₄@mesoporous-carbon monoliths, *Carbon* 167 (2020) 709–717, <https://doi.org/10.1016/j.carbon.2020.06.055>.